PLOS ONE

RESEARCH ARTICLE

Influence of Chirality of Crizotinib on Its MTH1 Protein Inhibitory Activity: Insight from Molecular Dynamics Simulations and Binding Free Energy Calculations

Yuzhen Niu[1], Dabo Pan[1], Danfeng Shi[1], Qifeng Bai[1], Huanxiang Liu[2,4], Xiaojun Yao[1,3]*

1 State Key Laboratory of Applied Organic Chemistry and Department of Chemistry, Lanzhou University, Lanzhou, 730000, China, **2** School of Pharmacy, Lanzhou University, Lanzhou, 730000, China, **3** Key Lab of Preclinical Study for New Drugs of Gansu Province, Lanzhou University, Lanzhou, 730000, China, **4** The Separating Scientific Institute of Lanzhou, Lanzhou, 730000, China

* xjyao@lzu.edu.cn

OPEN ACCESS

Citation: Niu Y, Pan D, Shi D, Bai Q, Liu H, Yao X (2015) Influence of Chirality of Crizotinib on Its MTH1 Protein Inhibitory Activity: Insight from Molecular Dynamics Simulations and Binding Free Energy Calculations. PLoS ONE 10(12): e0145219. doi:10.1371/journal.pone.0145219

Editor: Dennis Salahub, University of Calgary, CANADA

Received: March 20, 2015

Accepted: November 30, 2015

Published: December 17, 2015

Data Availability Statement: All relevant data are within the paper.

Funding: This work was supported by the National Natural Science Foundation of China (Grant No. 21475054) and the Fundamental Research Funds for the Central Universities (Grant No. lzujbky-2014-191). The funders had no role in study design, data collection and analysis, decision to publish, or preparation of the manuscript.

Competing Interests: The authors have declared that no competing interests exist.

Abstract

As a promising target for the treatment of lung cancer, the MutT Homolog 1 (MTH1) protein can be inhibited by crizotinib. A recent work shows that the inhibitory potency of (S)-crizotinib against MTH1 is about 20 times over that of (R)-crizotinib. But the detailed molecular mechanism remains unclear. In this study, molecular dynamics (MD) simulations and free energy calculations were used to elucidate the mechanism about the effect of chirality of crizotinib on the inhibitory activity against MTH1. The binding free energy of (S)-crizotinib predicted by the Molecular Mechanics/Generalized Born Surface Area (MM/GBSA) and Adaptive biasing force (ABF) methodologies is much lower than that of (R)-crizotinib, which is consistent with the experimental data. The analysis of the individual energy terms suggests that the van der Waals interactions are important for distinguishing the binding of (S)-crizotinib and (R)-crizotinib. The binding free energy decomposition analysis illustrated that residues Tyr7, Phe27, Phe72 and Trp117 were important for the selective binding of (S)-crizotinib to MTH1. The adaptive biasing force (ABF) method was further employed to elucidate the unbinding process of (S)-crizotinib and (R)-crizotinib from the binding pocket of MTH1. ABF simulation results suggest that the reaction coordinates of the (S)-crizotinib from the binding pocket is different from (R)-crizotinib. The results from our study can reveal the details about the effect of chirality on the inhibition activity of crizotinib to MTH1 and provide valuable information for the design of more potent inhibitors.

Introduction

MutT Homolog 1(MTH1), a nucleotide pool sanitizing enzyme, is a new therapeutic target in RAS-driven lung cancer reported recently [1]. MTH1 belongs to the Nudix hydrolase superfamily, characterized by a conserved 23-residue sequence segment (GX5EX7REUXEEXGU, U = I, L or V) [2]. MTH1 can implicate oncogenic KRAS-driven transformation of lung

epithelial cells, evade oxidative DNA damage-mediated induction of cellular senescence, and maintain optimal oncogene levels in KRAS-mutant NSCLC cells that are refractory to senescence induction [3, 4]. Oncogenic KRAS can promote production of reactive oxygen (ROS) [5–7], which can attack almost all biological molecules, such as DNA and protein, and produce a variety of negative effects. Previous study has demonstrated that normal cells do not need MTH1, but cancer cells, due to high level of ROS, need MTH1 to survive [8]. Selective inhibition of MTH1 by small molecules leads to DNA damage and suppresses cancer growth effectively, thus revealing MTH1 as a promising target for anticancer therapies [1, 9].

By using a chemical proteomics strategy, Kilian and colleagues confirmed that the kinase inhibitor crizotinib can inhibit MTH1 at nanomolar level [1]. Crizotinib is an oral small-molecule inhibitor of anaplastic lymphoma kinase (ALK) approved by US Food and Drug Administration (FDA) for the treatment of advanced non-small cell lung cancer (NSCLC) with ALK rearrangements [10]. The study reported by Kilian *et al.* shows that the clinically used (R)-enantiomer of crizotinib is almost inactive (IC_{50} = 1375nM) but (S)-crizotinib is a low nanomolar MTH1 inhibitor (IC_{50} = 72nM) [1]. Understanding about how the chirality influences the binding between crizotinib and MTH1 should be valuable to elucidate the inhibition and enantiomer-selectivity mechanism, and further provide some clues for the design of more potent inhibitors of MTH1.

The efficacy of a drug is not only associated with thermodynamics but also related to the binding kinetics between the drug and a defined target. The thermodynamics method such as Molecular Mechanics/Generalized Born Surface Area (MM/GBSA) [11–14] can provide the information about the drug binding affinity, while the free energies calculated by the adaptive biasing force (ABF) [15] can provide information about ligand–receptor binding kinetics. The combination use of binding free energy calculations by MM/GBSA and ABF should provide much useful information to understand the inhibition and enantiomer-selectivity mechanism of MTH1. In this study, the molecular mechanism of the binding processes of (S)-crizotinib and (R)-crizotinib to MTH1 were studied by molecular dynamics (MD) simulations, Molecular Mechanics/Generalized Born Surface Area (MM/GBSA) free energy calculations. The adaptive biasing force (ABF) technique was further employed to elucidate the difference of the unbinding pathways of the (R)- and (S)-crizotinib from the binding pocket of MTH1. We expect that this work would provide more details about the influence of chirality of crizotinib on the MTH1 inhibition activity and provide valuable information for the future design of more potent selective MTH1 inhibitors.

Materials and Methods

Simulation systems preparation

The initial 3-D coordinates of the (S)-crizotinib/MTH1 and (R)-crizotinib/MTH1 complexes were retrieved from the Protein Data Bank (PDB ID: 4C9X and 4C9W) [1]. The piperidine of the Crizotinib molecule in the (R)-crizotinib/MTH1 complex (PDB ID: 4C9W) was built by overlaying the piperidine group of (S)-crizotinib onto the (R)-crizotinib. It is important to note that in the structure of (S)-crizotinib/MTH1 (PDB ID: 4C9X), the residue Asn33 has only one conformer. Since usually Asn has two conformers, we used the one that has the same conformation to the crystal conformer. The Phe27 of MTH1 in (R)-crizotinib/MTH1 complex (PDB ID: 4C9W) was built by the *Protein Preparation Wizard* in Schrodinger 2009 [16]. We also used *Protein Preparation Wizard* to add side chain of residues, hydrogen atoms, assign protonation states, and relax the amino residue side chains of the proteins. The partial charges of the inhibitors were derived by using the restrained electrostatic potential (RESP) [17–19] fitting procedure based on the electrostatic potentials calculated by Hartree-Fock (HF) method with

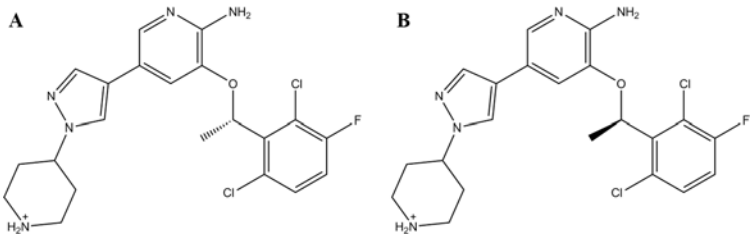

Fig 1. The structures of (S)-crizotinib (A) and (R)-crizotinib (B).

doi:10.1371/journal.pone.0145219.g001

6-31G (d) basis set in the Gaussian09 package [20]. The values of partial charges for (S)-crizotinib, and (R)-crizotinib were listed in S1 Table and S2 Table. The general AMBER force field (GAFF) [21] and AMBER03 force field (ff03) [22] were used for the inhibitors and proteins, respectively. Then, the two starting structures were placed in an orthorhombic periodic box of TIP3P water molecules [23], with a separation margin from the solute of 10 Å in each dimension.

Conventional molecular dynamics simulations

MD simulations of (S)-crizotinib (Fig 1A) and (R)-crizotinib (Fig 1B) in complex with MTH1 were performed by using NAMD 2.9 simulation package [24]. Long-range electrostatic interactions were handled by the Particle Mesh Ewald (PME) algorithm [25], while the short-range nonbonded interactions were calculated based on a cutoff of 10 Å. A steepest-descent minimization scheme was initially applied to the systems for 40000 steps, and then the systems were gradually heated in the NVT ensemble from 0 to 310 K in 100 ps by applying weak harmonic restraints with a constant force of 10 kcal/mol·Å^2 on the C and N atoms of the protein backbone. Then, the restrain was gradually decreased within 0.9 ns from 10 to 0.01 kcal/mol·Å^2. Finally, 20 ns MD simulations at a temperature of 310 K and a pressure of 1 atm. were carried out without any restrain. All bonds involving hydrogen atoms were restrained using the SHAKE [26] algorithm, and the time step was set to 2 fs.

Binding free energy calculations

The binding free energies of (S)-crizotinib and (R)-crizotinib to the MTH1 protein were predicted by the MM/GBSA method [27] in AMBER10 [28, 29] since it gives better ranking capabilities for binding affinities than Molecular Mechanics/Poisson-Boltzmann Surface Area (MM/PBSA) for most cases [30–32]. The first step of MM/GBSA is to generate a number of snapshots extracted from the stable MD production trajectory of the complex. Here, 500 snapshots were extracted from the last 10ns MD trajectory (repeated sampling 10 times). For each snapshot, the ligand binding free energy is estimated by the following equation:

$$< \Delta G_{bind} >=< \Delta H_{MM} > + < \Delta G_{solvation} > - T < \Delta S_{MM} > \quad (1)$$

Where $<\Delta G_{\mathrm{bind}}>$ is the calculated average free energy, and $<\Delta E_{\mathrm{MM}}>$ is the average molecular mechanical energy.

$$< \Delta E_{MM} >=< \Delta E_{bond} > + < \Delta E_{angle} > + < \Delta E_{tors} > + < \Delta E_{vdW} > + < \Delta E_{elec} > \quad (2)$$

$$< \Delta G_{solvation} >=< \Delta G_{GB} > + < \Delta G_{SA} > \quad (3)$$

Where these correspond to the bond, angle, torsion, vander Waals, and electrostatic terms in the molecular mechanical force field evaluated with no nonbonded cutoff. $<\Delta G_{\mathrm{solvation}}>$ is

the desolvation free energy upon ligand binding, and it can be decomposed into polar ($<\Delta G_{GB}>$) and nonpolar contributions ($<\Delta G_{SA}>$); The polar contribution of desolvation ($<\Delta G_{GB}>$) was calculated based on Generalized Born (GB) model (igb = 2) [33]. The dielectric constants for solute and solvent were set to 1 and 80, respectively. The nonpolar contribution of desolvation ($<\Delta G_{SA}>$) was determined by solvent accessible surface area (SASA) using the LCPO method [34]: $\Delta G_{SA} = 0.0072 \times \Delta SASA$. The conformational entropy contribution ($-T<\Delta S>$) upon ligand binding was calculated using normal-mode analysis [35–38] in the AMBER program. The contributions of entropy to binding free energy arise from changes of the translational, rotational, and vibrational degrees of freedom, defined as follows

$$S = S_{translational} + S_{rotaional} + S_{vibrational} \quad (4)$$

In the normal-mode analysis, the frequencies of the normal modes are calculated from a molecular mechanics force field using the Hessian matrix of second energy derivatives in terms of the force constants for each type of interaction. All minimizations and normal-mode calculations were performed with a distance-dependent dielectric function 4Rij (the distance between two atoms) to mimic solvent screening. The structures were further minimized with no cutoff for nonbonded interactions by using conjugate gradient and then Newton–Raphson minimizations until the RMS of the elements in the gradient vector was less than 10^{-4} kcal/(mol·Å). Due to the high computational cost in the entropy calculation, only 50 snapshots were extracted from the last 5ns MD trajectory were used to calculate the entropic contribution.

Per-residue free energy decomposition analysis

To identify the key residues responsible for the crizotinib binding process, the interaction between ligand and each residue was computed by using the MM/GBSA decomposition process in AMBER10 [28, 29]. All energy components were calculated using the 500 snapshots extracted from the last 5 ns MD trajectory. The binding interaction for each residue–inhibitor pair includes four terms: van der Waals contribution ($<\Delta G_{vdW}>$), electrostatic contribution ($<\Delta G_{ele}>$), polar solvation contribution ($<\Delta G_{GB}>$), and nonpolar solvation contribution ($<\Delta G_{SA}>$):

$$< \Delta G_{residue-inhibitor} >=< \Delta G_{vdW} > + < \Delta G_{ele} > + < \Delta G_{GB} > + < \Delta G_{SA} > \quad (5)$$

Adaptive biasing force simulations

The adaptive biasing force(ABF) method [15, 39, 40] developed by Darve *et al.* has been widely used in identifying reaction path coordinates[41, 42] and calculating free energy[16, 42, 43]. To carry out ABF simulations, an external biasing force, estimated locally from the sampled conformations of the system, is applied at each step to facilitate the biased molecule in overcoming significant energy barriers along the reaction coordinate (RC). The advantage of ABF is that the sampling of an order parameter or a low-dimensional hyper surface becomes uniform rapidly, which in turn greatly improves the statistical precision of the calculated free energy. Therefore, in this work, we used the ABF method to explore the change of the potentials of mean force (PMF) of (S)-crizotinib and (R)-crizotinib escaped from the MTH1 active pocket along the RC (Z-axis). The PMF depth (ΔW_{PMF}) [44–46], which can be obtained by $\Delta W_{PMF\text{-}lowest}$ -$\Delta W_{PMF\text{-}highest}$, was directly extracted from the ABF simulations based on 18-23Å of the reaction coordinates. The egress routes for (S)-crizotinib and (R)-crizotinib from the buried protein binding pocket of MTH1 were defined by the distance between N of Asp119

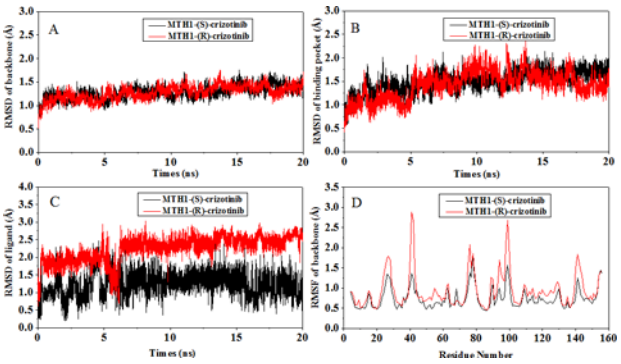

Fig 2. The monitoring of MD trajectories. (A) Time evolution of the RMSD of all protein backbone atoms; (B) Time evolution of the RMSD of Cα atoms for the residues around 5 Å of ligand; (C) Time evolution of the RMSD of heavy atoms for the ligand; (D) Time evolution of the RMSF of Cα atoms of the protein. The values reflect the equilibration of each of the systems relative to the initial structures.

doi:10.1371/journal.pone.0145219.g002

and C10 of (S)-crizotinib or (R)-crizotinib. In order to remove the effect of initial structures to the exit paths, five snapshot structures extracted from the last 5 ns equilibrium trajectories were used as the starting structures for the ABF simulations by using the same parameter set. The direction of the RC was rotated to the Z-axis. The initial structures were solvated again in a truncated octahedron box of TIP3P water molecules with a margin distance of 15Å. Prior to the ABF simulations, 1ns MD simulations were performed in the NPT ensemble (P = 1atm and T = 310K) to equilibrate the water molecules and ions with the receptor and ligand restrained with 1.0 kcal/mol.Å^2. In the ABF simulations, the residues out of 10 Å of the ligand were restrained with 5 kcal/mol.Å^2 to guarantee the direction of the RC. The length of the RC was separated into 23 windows with 1 Å/window and 0.1 Å/bin (10bin/window). Upper and lower wall constants were both set to 100 kcal/mol.A^2 in high barrier regions and low barrier regions to ensure full sampling. The *fullsamples* parameter was set to 1000 at each window prior to biasing. 4 and 3 ns MD simulations were performed for each window, which guaranteed the reliability of predicting the unbinding pathway by using the ABF method and the convergence of the PMF as shown in S2 Fig. A total of 736 ns MD simulations were performed for the two systems (368 ns for each system).

Results and Discussion

Structural flexibility and stability of the simulation systems

The conformational stabilities of the (S)-crizotinib MTH1 and (R)-crizotinib MTH1 complexes were monitored by the root-mean-square deviation (RMSD) values of the C_α atoms of MTH1, the heavy atoms of the ligand and the root mean square fluctuations (RMSFs) relative to their initial minimized structures. As shown in Fig 2, after 7ns, the RMSDs of the both systems tend to converge [47], indicating that the systems are stable and equilibrated. The (R)-crizotinib/MTH1 complex shows higher fluctuations than the (S)-crizotinib/MTH1 complex, with the averaged RMSDs of 1.35 and 2.48 Å for protein and ligand, respectively. Moreover, fluctuation of the active site for (R)-crizotinib is more significant than that for (S)-crizotinib.

The RMSFs from the initial structure of the MTH1 backbone atoms over the MD simulations is shown in Fig 2D. The RMSF analysis of each residue highlighted that the loop connecting the residues 23–32, 38–44, 88–101 and140-144 is the most flexible region.

It is worth noting that the side chains of some important residues like Phe27 and Phe139 adopt different conformation when compared with the X-ray structure. S1 Fig shows the

superposition of the stable structure extracted from equilibrium trajectories with the X-ray structure. It can be seen that the backbone of stable MTH1 protein do not deviate much from the X-ray structure in the two complexes. As for the force field for the simulation of crizotinib, the works by Sun et al [41, 42] proved the successful use of GAFF force field for the simulation of crizotinib.

Binding free energy calculations by MM/GBSA and ABF

The predicted binding free energies (ΔG_{bind}) and the energy components of the (S)-crizotinib/MTH1 and (R)-crizotinib/MTH1 complexes computed by MM/GBSA are summarized in Table 1. The binding affinity of the (S)-crizotinib/MTH1 complex (-24.77 kcal/mol) predicted by MM/GBSA is obviously lower than that of the (R)-crizotinib/MTH1 complex (-14.60 kcal/mol). The order of the calculated binding free energies is consistent with that of the experimental IC_{50} data. According to Table 1, electrostatic energy(ΔE_{ele}) and van der Waals energy(ΔE_{vdw}) terms in the gas phase provide the major favorable contributions to the (S)-crizotinib and (R)-crizotinib MTH1 binding, whereas polar solvation energies (ΔG_{GB}) and -TΔS impair the binding. Furthermore, the nonpolar contribution (-52.84 kcal/mol), which is the sum of the ΔE_{ele} and $\Delta E_{vdw,}$ for (S)-crizotinib binding is obviously favorable than that (-50.69 kcal/mol) for the (R)-crizotinib binding. The van der Waals term, is more crucial than the electrostatic part for determining the chirality selectivity of crizotinib. As MM/GBSA calculations do not include entropic terms, we estimated the corresponding entropic contributions (-TΔS) upon binding of ligands and MTH1. The values are 15.07 kcal/mol for (S)-crizotinib/MTH1 complex and 21.62 kcal/mol for (R)-crizotinib/MTH1 complex suggesting that conformational change also plays an important role to protein-ligand interaction.

Table 2 illustrates that the binding free energies based on the PMF depth (ΔW_{PMF}) are the same with those respect to the corresponding system. It can be found that the ranking of the binding free energies predicted by these two protocols all agree well with the experimental IC_{50} data. Here, we estimate the standard deviation of the free energy by MM/GBSA and ABF methods by repeating multiple trajectories (Table 2), and we have reason to believe that this error may be caused by the different force fields used in the two protocols (the MM/GBSA method uses implicit solvent and the ABF method uses explicit solvent, respectively). Since the correct

Table 1. The binding free energies and individual energy terms of (S)-crizotinib and (R)-crizotinib to MTH1 predicted by MM/GBSA.

	(S)-crizotinib/MTH1	(R)-crizotinib/MTH1
Contribution	**Mean (kcal/mol)**	**Mean (kcal/mol)**
ΔE_{ele}	-154.17±0.80[c]	-189.30±1.50
ΔE_{vdw}	-46.43±0.03	-44.16±0.12
ΔG_{SA}	-6.41±0.12	-6.53±0.10
ΔG_{GB}	167.17±0.74	203.77±0.01
$\Delta G_{nonpolar}$[a]	-52.84±0.25	-50.69±0.20
ΔG_{polar}[b]	13.00±0.07	14.47±0.11
$\Delta G_{total,GB}$	-39.84±0.29	-36.22±0.41
-TΔS	15.07±0.21	21.62±0.47
$\Delta G_{bind,GB}$	-24.77±0.36	-14.60±0.62

[a] $G_{nonpolar} = \Delta E_{vdw} + \Delta G_{SA}$

[b] $G_{polar} = \Delta E_{ele} + \Delta G_{GB}$.

[C] standard deviations calculated through 10 times of repeated sampling from 10-20ns trajectory.

doi:10.1371/journal.pone.0145219.t001

Table 2. Binding free energies of (S)-crizotinib/MTH1 and (R)-crizotinib/MTH1 complexes by MM/GBSA and ABF.

Name	(S)-crizotinib/MTH1	(R)-crizotinib/MTH1
ΔG_{bind} (kcal/mol)	-24.77±0.36	-14.60±0.62
ΔG_{PMF} (kcal/mol)	-29.60±0.38[a]	-22.38±0.51
IC_{50}(nM)	72	1375

[a] standard deviation calculated based on 18-23Å reaction coordinates of the 5 replicas we simulated.

doi:10.1371/journal.pone.0145219.t002

ranking of the binding free energies is usually emphasized in molecular designs, it is reasonable to accept the results above.

We also calculated the strain energy [48] (the changes of the enthalpy of the ligand translating from the unbound conformation to bound conformation, calculated by MM-GBSA method) of (S)-crizotinib and (R)-crizotinib, the strain energy of (S)-crizotinib (1.08 kcal/mol) is lower than that of (R)-crizotinib (5.69 kcal/mol). The fluctuation of (R)-crizotinib heavy atom is larger than that of (S)-crizotinib (Fig 2C).

Decomposition of effective energies on a per residue basis

The binding free energies in the (S)-crizotinib/MTH1 or (R)-crizotinib/MTH1 complexes was decomposed into contribution of residues by using MM/GBSA approach. Comparison of the interactions spectra (Fig 3 and Table 3) shows that the selective binding between (S)-crizotinib and (R)-crizotinib to MTH1 is primarily determined by Tyr7, Phe27, Phe72 and Trp117. The contribution of Phe27 to the binding of (S)-crizotinib (-3.02 kcal/mol) is substantially stronger than that to (R)-crizotinib (-0.18 kcal/mol). Structural analysis provides a more deep insight into the basis of the selectivity (Fig 4). The conformation of the phenyl group of the side chain of Phe27 in the (R)-crizotinib/MTH1 complex is significantly different from that in the (S)-crizotinib/MTH1 complex. The phenyl group of the side chain of Phe27 in the (R)-crizotinib/MTH1 complex is far from the piperidine ring of (R)-crizotinib, implying that Phe27 forms more favorable contacts with (S)-crizotinib than (R)-crizotinib. To be more specific, this structural difference might explain the difference of the van der Waals interactions. For residue Trp117, its contribution to the (R)-crizotinib and (S)-crizotinib bindings are -2.56 kcal/mol

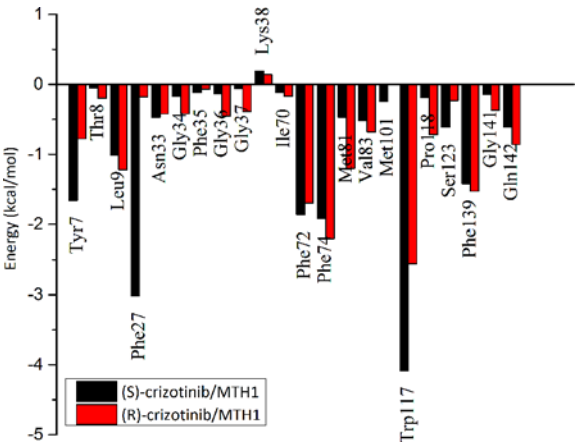

Fig 3. Intermolecular ligand receptor (MTH1) interaction spectrum of the MTH1-crizotinib complex according to the MM/GBSA analysis methods.

doi:10.1371/journal.pone.0145219.g003

Table 3. The contributions of the important residues for the ligand binding predicted by the MM/GBSA free energy decomposition (kcal/mol).

	(S)-crizotinib/MTH1				(R)-crizotinib/MTH1			
Residue	ΔE_{vdw}	ΔE_{ele}	ΔG_{sol}[a]	ΔG_{total}[b]	ΔE_{vdw}	ΔE_{ele}	ΔG_{sol}	ΔG_{total}
Tyr7	**-1.90**	**-0.40**	**-0.17**	**-1.66**	**-0.88**	**0.28**	**-0.18**	**-0.78**
Thr8	-0.10	-0.23	0.27	-0.05	-0.21	-0.48	0.48	-0.20
Leu9	-0.93	0.17	-0.26	-1.01	-1.15	0.34	-0.42	-1.22
Phe27	**-2.49**	**-0.50**	**-0.03**	**-3.02**	**-0.30**	**0.02**	**0.10**	**-0.18**
Asn33	-0.88	-0.31	0.72	-0.47	-0.84	0.57	-0.15	-0.42
Gly34	-0.21	-0.66	0.70	-0.17	-0.37	-1.17	1.12	-0.42
Phe35	-0.10	0.19	-0.21	-0.12	-0.25	0.30	-0.11	-0.07
Gly36	-0.14	0.10	-0.09	-0.13	-0.63	-0.06	0.24	-0.45
Gly37	-0.09	0.33	-0.30	-0.06	-0.37	-0.01	0.00	-0.39
Lys38	-0.04	12.6	-12.3	0.19	-0.07	10.9	-10.7	0.14
Ile70	-0.12	-0.24	0.24	-0.12	-0.17	-0.16	0.16	-0.17
Phe72	**-1.92**	**0.01**	**0.05**	**-1.86**	**-1.71**	**-0.29**	**0.30**	**-1.70**
Phe74	-1.73	0.12	-0.32	-1.92	-2.11	0.15	-0.24	-2.20
Met81	-0.49	-0.42	0.44	-0.47	-1.17	-0.05	0.01	-1.20
Val83	-0.43	-0.05	-0.05	-0.52	-0.62	-0.07	0.01	-0.68
Met101	-0.26	0.45	-0.43	-0.24	-0.02	0.29	-0.28	-0.01
Trp117	-4.24	0.26	-0.11	-4.09	-2.61	0.24	-0.18	-2.56
Pro118	-0.18	0.41	-0.42	-0.19	-0.64	0.30	-0.38	-0.72
Ser123	-0.73	0.14	-0.02	-0.61	-0.22	0.48	-0.49	-0.23
Phe139	-1.52	0.11	0.20	-1.42	-1.48	-0.39	0.34	-1.53
Gly141	-0.49	-2.04	2.39	-0.14	-0.47	-2.60	2.70	-0.37
Gln142	-1.00	-0.13	0.53	-0.16	-2.23	-2.71	4.08	-0.86

[a] ΔG_{sol}: Desolvation energy of residue to ligand binding

[b] ΔG_{total}: Total contribution of residue to ligand binding.

doi:10.1371/journal.pone.0145219.t003

and -4.09 kcal/mol, respectively. The favorable free energy contribution of Trp117 for (S)-crizotinib is mainly from the van der Waals interaction (-4.24 kcal/mol).

Difference in the binding free energies also occurs in Tyr7, with -1.66 and -0.78 kcal/mol for (S)-crizotinib and (R)-crizotinib. It can also see that the conformational change of the 2,6-dichloro-3-fluoro-phenyl of the (R)-crizotinib comparing to that of (S)-crizotinib and the

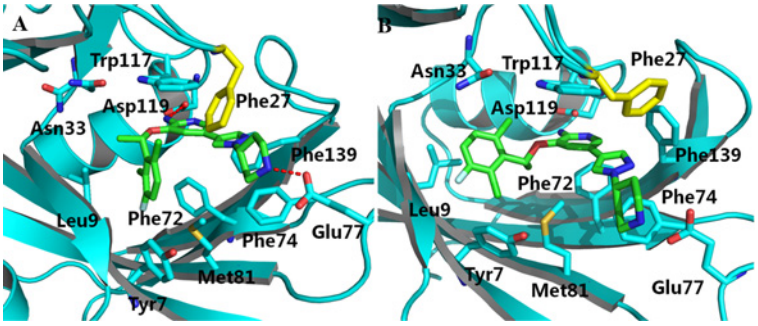

Fig 4. MD-simulated structures of (S)-crizotinib (A) and (R)-crizotinib (B) bound to the active site of the MTH1 protein. The protein is represented as blue cartoon, respectively. Blue stick representations are shown for residues in the active site. The green stick is the ligand. The important residue is illustrated in yellow stick in MTH1 protein. Red dashed lines represent the hydrogen bond.

doi:10.1371/journal.pone.0145219.g004

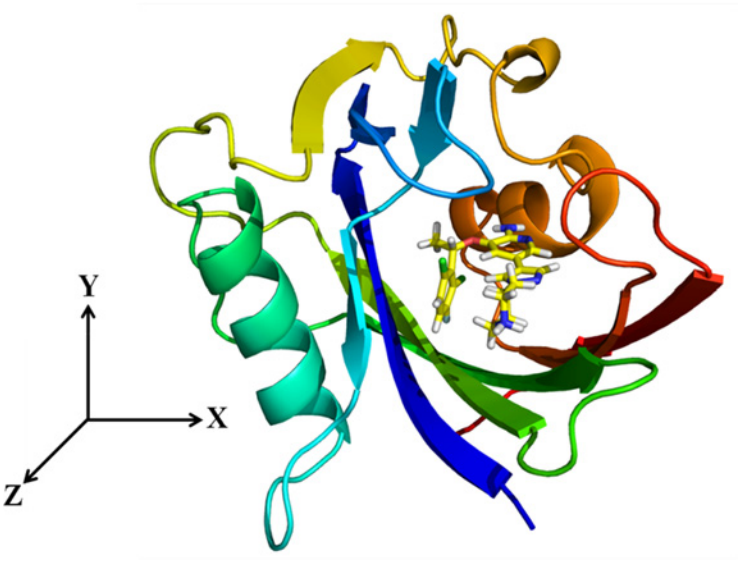

Fig 5. The MTH1 active pocket and the Z-axis is the direction of the ligand escape from the active pocket of MTH1.

doi:10.1371/journal.pone.0145219.g005

conformational change of Tyr7 in the (R)-crizotinib/MTH1 complex is larger than that in the (S)-crizotinib/MTH1 complex (Fig 2D). This is also in accordance with the fact that the favorable contribution is mainly from the van der Waals energy. It also further illustrates that Tyr7, Phe27, Phe72 and Trp117 are key residues in selective binding.

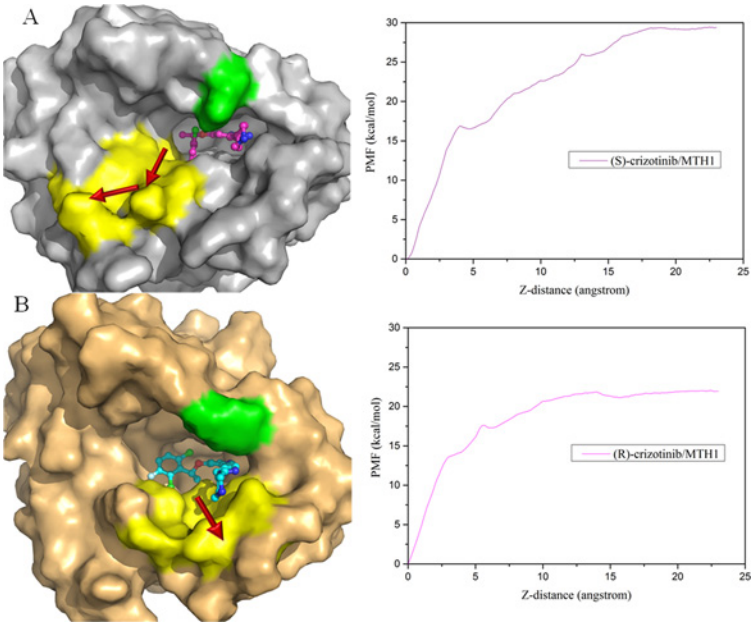

Fig 6. Initial structures of the ABF and the PMF curves of the (S)-crizotinib complex (A) and (R)-crizotinib complex (B). Red arrows represent the direction of the crizotinib escaping from the binding pocket. The yellow region denotes the necessary bin ding channel for (R)-crizotinib escaping out of the active pocket, and the green region represents the important residue Phe27 for the binding of (R)-crizotinib.

doi:10.1371/journal.pone.0145219.g006

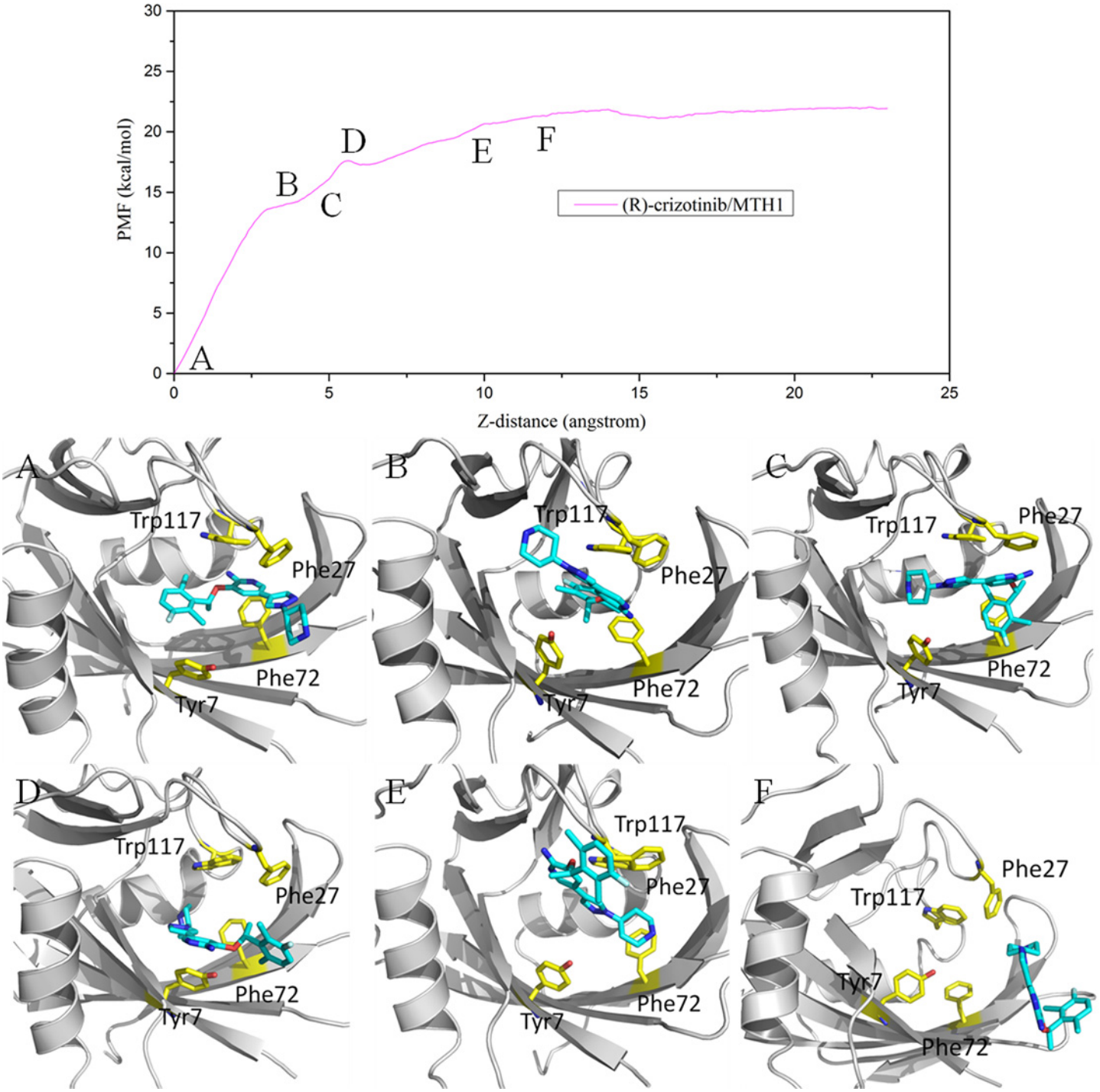

Fig 7. Conformation of (R)-crizotinib along the reaction coordinate (Z-axis) in the MTH1 protein. Top: the PMF along the reaction coordinate. Bottom: Corresponding representatives' structures of the (R)-crizotinib/MTH1. The proteins are shown in gray cartoon, respectively. Yellow stick representations are shown for important residues. The blue stick is the ligand.

doi:10.1371/journal.pone.0145219.g007

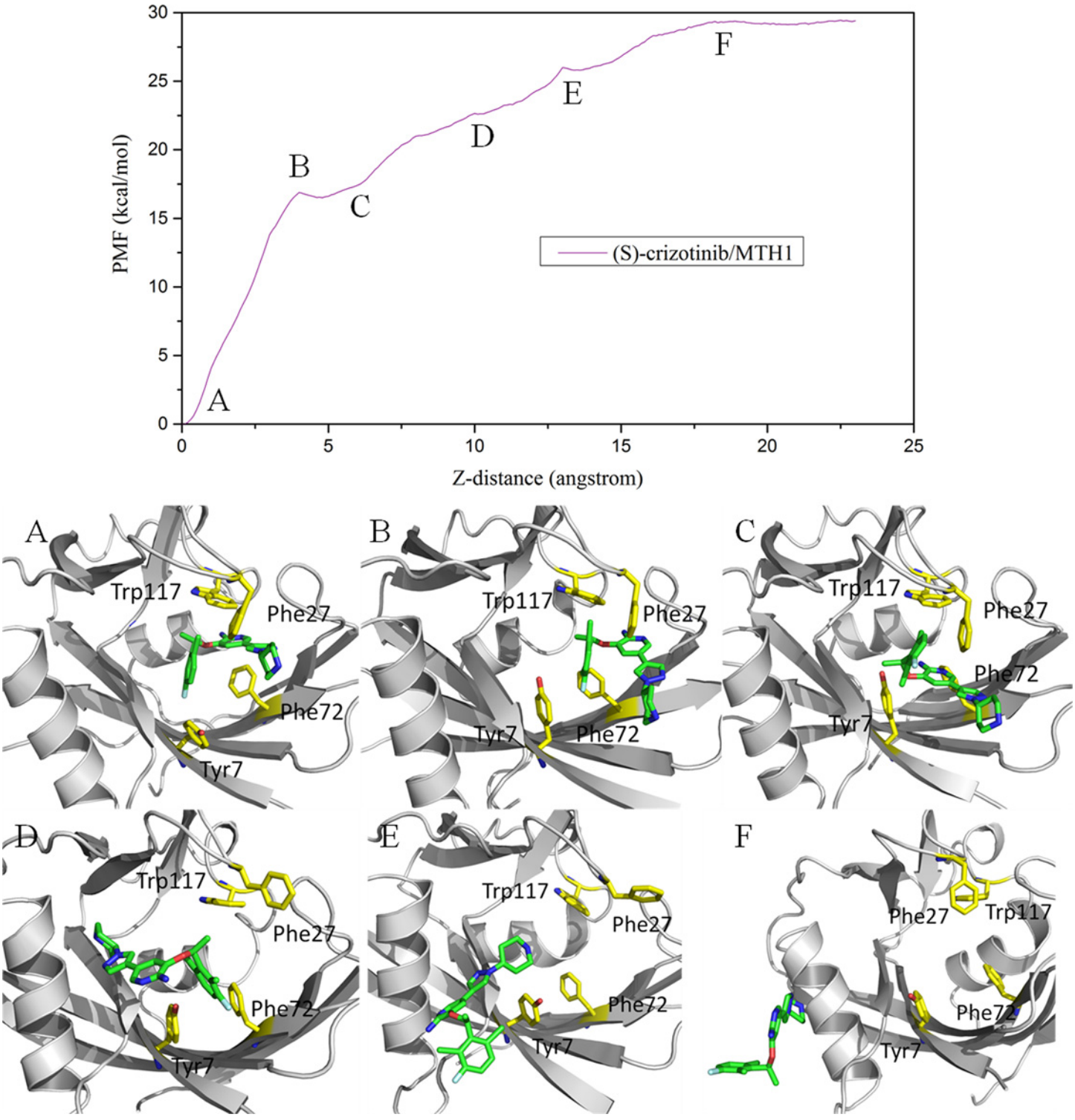

Fig 8. Conformation of (S)-crizotinib along the reaction coordinate (Z-axis) in the MTH1 protein. Top: the PMF along the reaction coordinate. Bottom: Corresponding representatives' structures of the (S)-crizotinib/MTH1. The proteins are shown in gray cartoon, respectively. Yellow stick representations are shown for important residues. The green stick is the ligand.

doi:10.1371/journal.pone.0145219.g008

Comparison of the PMFs along the Reaction Coordinates

As shown in Fig 5, the direction of the largest pocket was chosen as the RC, and it was rotated along Z-axis for the projection of the biasing force. The beginning of the RC for the determination of the PMF changes was defined as the distance between the center of mass of the ligand and the center of mass of the backbone of MTH1. During the simulations, the RC spanned to ~23.0 Å. Fig 6 shows the initial structures of the (S)-crizotinib/MTH1 and (R)-crizotinib/MTH1 complexes, and their corresponding PMF curves for the crizotinib unbinding process from the ABF simulations.

It can be seen that the PMF curves for the two systems are different: a platform of the PMFs was observed at ~12 Å of the RC for (R)-crizotinib, while for (S)-crizotinib, the platform is at ~18 Å. The free energy of unbinding for (S)-crizotinib is about 7 kcal/mol higher than that for (R)-crizotinib. The detailed processes of the (R)-crizotinib and (S)-crizotinib unbinding from the MTH1 are illustrated in Figs 7 and 8. As shown in Fig 7, (R)-crizotinib gradually moves from the binding pocket with the increase of the biasing potential added to (R)-crizotinib. At 12 Å of the RC, the biasing potential reaches the maximum value of ~22 kcal/mol and then becomes relatively stable. From Fig 7A–7E, we can see that (R)-crizotinib turns a somersault and then jumps out of the active pocket, which might be affected by the residues along the reaction direction.

As shown in Fig 8, for the (S)-crizotinib/MTH1 complex, before ~12 Å of the RC, the curve is similar to that of the (R)-crizotinib/MTH1 complex. After that the curve of the (S)-crizotinib/MTH1 complex rises continuously to ~18 Å of the RC around ~29 kcal/mol, while the (R)-crizotinib/MTH1complex already reaches a platform around ~22 kcal/mol. The gap between these two platforms is ~7 kcal/mol. It can be seen that Phe27 in the (S)-crizotinib/MTH1 complex narrow the entrance of the binding pocket and a V-like route was adopted by (S)-crizotinib to escape out of the binding pocket as shown in Fig 6A.

Conclusions

In this work, we investigated the influence of chirality of crizotinib on its MTH1 Inhibitory activity by the use of molecular dynamics simulations and binding free energy calculations. The comparison of the PMFs indicates (S)-crizotinib and (R)-crizotinib have different reaction coordinates when they escape from MTH1. The binding free energy calculations from MM/GBSA and ABF calculation method are in good agreement with the experimental data. Residue decomposition shows that the decrease of the binding energies for Tyr7, Phe27, Phe72 and Trp117 is primarily contributed from the conformation rearrangement of the MTH1 active site of the (R)-crizotinib. The residue Phe27 breaks the balance of (R)-crizotinib inside the binding pocket. Our studies are helpful to elucidate the chirality effect of crizotinib inhibition activity on MTH1 protein. These results are valuable for designing new novel MTH1 inhibitor in the future.

Supporting Information

S1 Fig. Superposition of the stable structure extracted from equilibrium trajectory with the X-ray structure. A. (S)-crizotinib/MTH1 protein complex; B. (R)-crizotinib/MTH1 protein complex.
(TIF)

S2 Fig. Convergence of the potentials of mean force (PMFs), and it is convergent.
(TIF)

S1 Table. Atom types and partial charges for (S)-crizotinib.
(DOC)

S2 Table. Atom types and partial charges for (R)-crizotinib.
(DOC)

Acknowledgments

This work was supported by the National Natural Science Foundation of China (Grant No. 21475054) and the Fundamental Research Funds for the Central Universities (Grant No. lzujbky-2014-191).

Author Contributions

Conceived and designed the experiments: YN XY. Performed the experiments: YN DP DS. Analyzed the data: YN DP DS QB HL. Contributed reagents/materials/analysis tools: YN DP DS QB HL. Wrote the paper: YN XY.

References

1. Huber KVM, Salah E, Radic B, Gridling M, Elkins JM, Stukalov A, et al. (2014) Stereospecific targeting of MTH1 by (S)-crizotinib as an anticancer strategy. Nature 508: 222–227. doi: 10.1038/nature13194 PMID: 24695225
2. Svensson LM, Jemth A-S, Desroses M, Loseva O, Helleday T, Hoegbom M, et al. (2011) Crystal structure of human MTH1 and the 8-oxo-dGMP product complex. FFBS Lett 585: 2617–2621.
3. Kennedy CH, Pass HI, Mitchell JB (2003) Expression of human MutT homologue (hMTH1) protein in primary non-small-cell lung carcinomas and histologically normal surrounding tissue. Free Radi Biol Med 34: 1447–1457.
4. Patel A, Burton DG, Halvorsen K, Balkan W, Reiner T, Perez-Stable C, et al. (2015) MutT Homolog 1 (MTH1) maintains multiple KRAS-driven pro-malignant pathways. Oncogene, 34:2586–2596. doi: 10.1038/onc.2014.195 PMID: 25023700
5. Arbiser JL, Petros J, Klafter R, Govindajaran B, McLaughlin ER, Brown LF, et al. (2002) Reactive oxygen generated by Nox1 triggers the angiogenic switch. Proc Natl Acad Sci USA 99: 715–720. PMID: 11805326
6. Mitsushita J, Lambeth JD, Kamata T (2004) The superoxide-generating oxidase Nox1 is functionally required for Ras oncogene transformation. Cancer Res 64: 3580–3585. PMID: 15150115
7. Weinberg F, Hamanaka R, Wheaton WW, Weinberg S, Joseph J, Lopez M, et al. (2010) Mitochondrial metabolism and ROS generation are essential for Kras-mediated tumorigenicity. Proc Natl Acad Sci USA 107: 8788–8793. doi: 10.1073/pnas.1003428107 PMID: 20421486
8. Rai P (2012) Human Mut T Homolog 1 (MTH1): a roadblock for the tumor-suppressive effects of oncogenic RAS-induced ROS. Small GTPases 3: 120–125. doi: 10.4161/sgtp.19556 PMID: 22790201
9. Gad H, Koolmeister T, Jemth A-S, Eshtad S, Jacques SA, Strom CE, et al. (2014) MTH1 inhibition eradicates cancer by preventing sanitation of the dNTP pool. Nature 508: 215–221. doi: 10.1038/nature13181 PMID: 24695224
10. Cui JJ, Tran-Dube M, Shen H, Nambu M, Kung PP, Pairish M, et al. (2011) Structure based drug design of crizotinib (PF-02341066), a potent and selective dual inhibitor of mesenchymal-epithelial transition factor (c-MET) kinase and anaplastic lymphoma kinase (ALK). J Med Chem 54: 6342–6363. doi: 10.1021/jm2007613 PMID: 21812414
11. Bello M (2014) Binding free energy calculations between bovine beta-lactoglobulin and four fatty acids using the MMGBSA method. Biopolymers 101: 1010–1018. doi: 10.1002/bip.22483 PMID: 24619557
12. Gaillard T, Simonson T (2014) Pairwise decomposition of an MMGBSA energy function for computational protein design. J Comput Chem 35: 1371–1387. doi: 10.1002/jcc.23637 PMID: 24854675
13. Srivastava HK, Sastry GN (2013) Efficient estimation of MMGBSA-based BEs for DNA and aromatic furan amidino derivatives. J Biomol Struct Dyn 31: 522–537. doi: 10.1080/07391102.2012.703071 PMID: 22877232
14. Ylilauri M, Pentikainen OT (2013) MMGBSA as a tool to understand the binding affinities of filamin-peptide interactions. J Chem Inf Model 53: 2626–2633. doi: 10.1021/ci4002475 PMID: 23988151

15. Darve E, Rodriguez-Gomez D, Pohorille A (2008) Adaptive biasing force method for scalar and vector free energy calculations. J Chem Phys 128: 144120. doi: 10.1063/1.2829861 PMID: 18412436
16. prime (2008) version 2.0. Schrödinger,LLC,New York.
17. Bayly CI, Cieplak P, Cornell W, Kollman PA (1993) A well-behaved electrostatic potential based method using charge restraints for deriving atomic charges: the RESP model. J Phys Chem 97: 10269–10280.
18. Cieplak P, Cornell WD, Bayly C, Kollman PA (1995) Application of the multimolecule and multiconformational RESP methodology to biopolymers: Charge derivation for DNA, RNA, and proteins. J Comput Chem 16: 1357–1377.
19. Fox T, Kollman PA (1998) Application of the RESP Methodology in the Parametrization of Organic Solvents. J Phys Chem B 102: 8070–8079.
20. M. J. Frisch GWT, H. B. Schlegel, G. E. Scuseria, M. A. Robb, J., R. Cheeseman GS, V. Barone, et al. Gaussian 09; Gaussian, Inc.: Wallingford, CT, 2009.
21. Wang J, Wolf RM, Caldwell JW, Kollman PA, Case DA (2004) Development and testing of a general amber force field. J Comput Chem 25: 1157–1174. PMID: 15116359
22. Duan Y, Wu C, Chowdhury S, Lee MC, Xiong G, Zhang W, et al. (2003) A point-charge force field for molecular mechanics simulations of proteins based on condensed-phase quantum mechanical calculations. J. Comput Chem 24: 1999–2012. PMID: 14531054
23. Jorgensen WL, Chandrasekhar J, Madura JD, Impey RW, Klein ML (1983) Comparison of simple potential functions for simulating liquid water. J Chem Phys 79: 926–935.
24. Phillips JC, Braun R, Wang W, Gumbart J, Tajkhorshid E, Villa E, et al. (2005) Scalable molecular dynamics with NAMD. J. Comput Chem 26: 1781–1802. PMID: 16222654
25. Darden T, York D, Pedersen L (1993) Particle mesh Ewald: An N·log(N) method for Ewald sums in large systems. J Chem Phys 98: 10089–10092.
26. Ryckaert J-P, Ciccotti G, Berendsen HJC (1977) Numerical integration of the cartesian equations of motion of a system with constraints: molecular dynamics of n-alkanes. J Comput Phys 23: 327–341.
27. Kollman PA, Massova I, Reyes C, Kuhn B, Huo S, Chong L, et al. (2000) Calculating structures and free energies of complex molecules: combining molecular mechanics and continuum models. Acc Chem Res 33: 889–897. PMID: 11123888
28. Hou T, Zhang W, Case DA, Wang W (2008) Characterization of domain-peptide interaction interface: A case study on the amphiphysin-1 SH3 domain. J Mol Biol 376: 1201–1214. doi: 10.1016/j.jmb.2007.12.054 PMID: 18206907
29. Gohlke H, Kiel C, Case DA (2003) Insights into protein-protein binding by binding free energy calculation and free energy decomposition for the Ras-Raf and Ras-RalGDS complexes. J Mol Biol 330: 891–913. PMID: 12850155
30. Hou T, Wang J, Li Y, Wang W (2011) Assessing the Performance of the MM/PBSA and MM/GBSA Methods. 1. The Accuracy of Binding Free Energy Calculations Based on Molecular Dynamics Simulations. J Chem Inf Model 51: 69–82. doi: 10.1021/ci100275a PMID: 21117705
31. Sun H, Li Y, Tian S, Xu L, Hou T (2014) Assessing the performance of MM/PBSA and MM/GBSA methods. 4. Accuracies of MM/PBSA and MM/GBSA methodologies evaluated by various simulation protocols using PDBbind data set. Phys Chem Chem Phys 16: 16719–16729. doi: 10.1039/c4cp01388c PMID: 24999761
32. Hou T, Wang J, Li Y, Wang W (2011) Assessing the Performance of the Molecular Mechanics/Poisson Boltzmann Surface Area and Molecular Mechanics/Generalized Born Surface Area Methods. II. The Accuracy of Ranking Poses Generated From Docking. J Comput Chem 32: 866–877. doi: 10.1002/jcc.21666 PMID: 20949517
33. Onufriev A, Bashford D, Case DA (2004) Exploring protein native states and large-scale conformational changes with a modified generalized born model. Proteins 55: 383–394. PMID: 15048829
34. Weiser J, Shenkin PS, Still WC (1999) Approximate atomic surfaces from linear combinations of pairwise overlaps (LCPO). J Comput Chem 20: 217–230.
35. Case DA (1994) Normal mode analysis of protein dynamics. Curr Opin Struct Biol 4: 285–290.
36. Case DA (2002) Molecular dynamics and normal mode analysis of biomolecular rigidity. Rigidity theory and applications. Springer. pp. 329–344.
37. Case DA, Cheatham TE, Darden T, Gohlke H, Luo R, Merz KM, et al. (2005) The Amber biomolecular simulation programs. J Comput Chem 26: 1668–1688. PMID: 16200636
38. Sundberg EJ, Mariuzza RA (2002) Molecular recognition in antibody-antigen complexes. Adv Protein Chem 61: 119–160. PMID: 12461823

39. Faller CE, Reilly KA, Hills RD Jr, Guvench O (2013) Peptide backbone sampling convergence with the adaptive biasing force algorithm. J Phys Chem B 117: 518–526. doi: 10.1021/jp309741j PMID: 23215032

40. Rodriguez-Gomez D, Darve E, Pohorille A (2004) Assessing the efficiency of free energy calculation methods. J Chem Phys 120: 3563–3578. PMID: 15268518

41. Sun H, Li Y, Tian S, Wang J, Hou T (2014) P-loop conformation governed crizotinib resistance in G2032R-mutated ROS1 tyrosine kinase: clues from free energy landscape. PLoS Comput Biol 10: e1003729. doi: 10.1371/journal.pcbi.1003729 PMID: 25033171

42. Sun H, Li Y, Li D, Hou T (2013) Insight into Crizotinib Resistance Mechanisms Caused by Three Mutations in ALK Tyrosine Kinase using Free Energy Calculation Approaches. J Chem inf model 53: 2376–2389. doi: 10.1021/ci400188q PMID: 23952683

43. Martin HS, Jha S, Coveney PV (2014) Comparative analysis of nucleotide translocation through protein nanopores using steered molecular dynamics and an adaptive biasing force. J Comput Chem 35: 692–702. doi: 10.1002/jcc.23525 PMID: 24403093

44. Deng Y, Roux B (2009) Computations of standard binding free energies with molecular dynamics simulations. J Phys Chem B 113: 2234–2246. doi: 10.1021/jp807701h PMID: 19146384

45. Gumbart JC, Roux B, Chipot C (2013) Standard binding free energies from computer simulations: What is the best strategy? J Chem Theory Comput 9: 794–802. PMID: 23794960

46. Woo HJ, Roux B (2005) Calculation of absolute protein-ligand binding free energy from computer simulations. Proc Natl Acad Sci USA 102: 6825–6830. PMID: 15867154

47. Romo TD, Grossfield A (2011) Block covariance overlap method and convergence in molecular dynamics simulation. J Chem Theory Comput 7: 2464–2472. PMID: 26606620

48. George P, Trachtman M, Bock CW, Brett AM (1976) An alternative approach to the problem of assessing destabilization energies (strain energies) in cyclic hydrocarbons. Tetrahedron 32: 317–323.